

Article

In Situ Polymerization to Boron Nitride-Fluorinated Poly Methacrylate Composites as Thin but Robust Anti-Corrosion Coatings

Qingqing Hu ¹, Aijuan Lv ¹, Yukang Ma ¹, Yan Wang ¹, Haoyi Zhang ¹, Xin Mi ² and Qiang Xiao ^{1,*}

¹ Key Laboratory of the Ministry of Education for Advanced Catalysis Materials, Institute of Advanced Fluorine-Containing Materials, Zhejiang Normal University, Jinhua 321004, China; huqingqing@zjnu.edu.cn (Q.H.); lvaijuan@zjnu.edu.cn (A.L.); CopeeM@zjnu.edu.cn (Y.M.); wangyan1618@zjnu.edu.cn (Y.W.); zhanghy@zjnu.edu.cn (H.Z.)

² Beijing Thinvec Co. Ltd., Beijing 100176, China; technical@thinvec.com

* Correspondence: xiaoq@zjnu.edu.cn

Abstract: High-performance anti-corrosion coatings featuring easy processability and thin thickness are highly desired in industry. Yet, solution process coating often faces a sedimentation problem with particles which are used as reinforcement in coatings. In this contribution, boron nitride (BN) was modified by an acrylate silane coupling agent (KH-570) to obtain acrylated BN flakes. Afterwards, the acrylated BN flakes were in situ copolymerized with 2-(perfluorohexyl)ethyl methacrylate to synthesize BN-fluorinated poly methacrylate (PFBP) composites. The as-obtained PFBP composites can form stable coating solutions, in which sedimentation of BN flakes seldom happens. The coating solution can easily form uniform coatings on various substrates with nanoscale thickness, confirmed by scanning electron microscope (SEM). The corrosion resistance of the samples coated PFBP coatings in 3.5 wt.% sodium chloride solution was evaluated by electrochemical impedance spectroscopy (EIS). It is indicated that the incorporation of BN flakes greatly reduce the corrosion rate. Adhesion measurements and abrasion resistance test indicate the PFBP coating performs good adhesion to substrate and robustness. Through the in situ polymerization, acrylated BN flakes are connected with the polymer chain, which inhibits the sedimentation of BN in the coating solution. Additionally, the BN flakes dispersed in the fluorinated polymer act as barriers, improving the corrosion resistance of the coated samples.

Keywords: in situ polymerization; boron nitride; corrosion resistant; coating; fluorinated poly-methacrylate; anti-moisture



Citation: Hu, Q.; Lv, A.; Ma, Y.; Wang, Y.; Zhang, H.; Mi, X.; Xiao, Q. In Situ Polymerization to Boron Nitride-Fluorinated Poly Methacrylate Composites as Thin but Robust Anti-Corrosion Coatings. *Coatings* **2021**, *11*, 1518. <https://doi.org/10.3390/coatings11121518>

Academic Editor: Kyong Yop Rhee

Received: 1 November 2021

Accepted: 3 December 2021

Published: 10 December 2021

Publisher's Note: MDPI stays neutral with regard to jurisdictional claims in published maps and institutional affiliations.



Copyright: © 2021 by the authors. Licensee MDPI, Basel, Switzerland. This article is an open access article distributed under the terms and conditions of the Creative Commons Attribution (CC BY) license (<https://creativecommons.org/licenses/by/4.0/>).

1. Introduction

Anti-moisture and anti-corrosion for the metallic components are highly desirable in industry. Coating with polymeric film is one of the most effective and convenient methods to prevent the corrosion of metal. Through forming a water-repellent coating film as a barrier, polymer coatings protect the metal surface from corrosion [1]. At present, the protective polymeric coatings widely used in the electronic industry include fluorine-containing resin, epoxy resin, phenolic resin, etc. [2]. Among them, fluorine-containing resin features low surface energy, low water absorption, high hydrophobicity and high stability [3,4]. Compared to the widely used fluorinated resins, e.g., polytetrafluoroethylene (PTFE), which can be hardly dissolved in solvent, fluorinated polyacrylate is soluble in some fluorinated solvents, resulting in an ease of processability in forming films on substrate [5–7]. The coatings with high performance usually rely on high barrier property and good adhesion to substrate. Reinforcement with nanomaterials could improve the anticorrosion property of fluorinated polymer by inhibiting the permeation of corrosion media and forming superhydrophobic surface [7,8]. In recent years, the rise of graphene has aroused

people's attention in the field of anticorrosion [9]. By virtue of the large high aspect ratio and impermeability to gases, graphene holds promise as an effective anticorrosion barrier when incorporated in anticorrosive coatings [10–13]. However, the high conductivity of graphene limits its long-term application in the protection of electronic products [14].

Boron nitride (BN), which has a layered structure similar to graphene, features high resistivity, excellent thermal conductivity and high impermeability [15–18]. Shen et al. demonstrated that monolayer BN exhibited much better long-term corrosion barrier performance than graphene [14]. Jiang et al. reported an in situ synthesis of BN coatings on substrates, which can effectively prevent the substrates from being oxidized or corrosion [19]. BN could also be added in polymeric coatings as filler, finding an improvement of anti-corrosion performance. Husain et al. illustrated that h-BN/PVA hybrid coatings showed an improved corrosion protection against simulated seawater media [20]. Additionally, incorporation into epoxy resin (EP) has verified BN is a good reinforcement material. To improve the compatibility of BN and the EP, non-covalent modification of BN has been made with various chemicals such as polydopamine (PDA) [21], carboxylated aniline trimer (CAT) [22] and tannins acid (TA) [23,24], etc. Oh et al. prepared BN/polymethyl methacrylate (PMMA) composites with high thermal conductivity using an in situ polymerization process. BN was bonded with vinyltriethoxysilane to introduce double bonds, and it was directly linked with the PMMA chains during the polymerization step. The BN/PMMA composites exhibited an obvious thermal conductivity enhancement, with a value that was 17.8 times higher than that of PMMA [25]. Very recently, He et al. initiated an in situ anionic polymerization of methyl methacrylate on the exfoliated BN nanosheets. The PMMA chains grafted on the BN nanosheets enhanced the solubility in solvent [26].

From the above, a great deal of work relating to the incorporation of layered materials (graphene, BN, etc.) into polymer coatings has been reported. However, seldom has work been focused on the incorporation of these layered materials into fluorinated polymethacrylate systems. In a fluorous composite coating system, which has low viscosity, sedimentation of the incorporated layered materials can hardly be avoided.

In this contribution, BN powder was firstly exfoliated to flakes using a wet ball-milling method followed by modification of 3-(trimethoxysilyl)propyl methacrylate (KH-570). Then, the acrylated BN flakes was in situ polymerized with 2-(perfluorohexyl)ethyl methacrylate (C6Rf) to obtain BN-fluorinated poly methacrylate (PFBP) composites by a precipitation polymerization method. The PFBP composites can be well dissolved in a fluorous solvent forming a stable suspension. BN flakes are covalently bonded to the polymer matrix, which on one hand, eliminates the possible appearance of voids between BN flakes and polymer; on the other hand, inhibits the sedimentation of BN from the coating solution. BN flakes are well dispersed in the polymer matrix and the formed PFBP coatings display greatly enhanced corrosion resistance property.

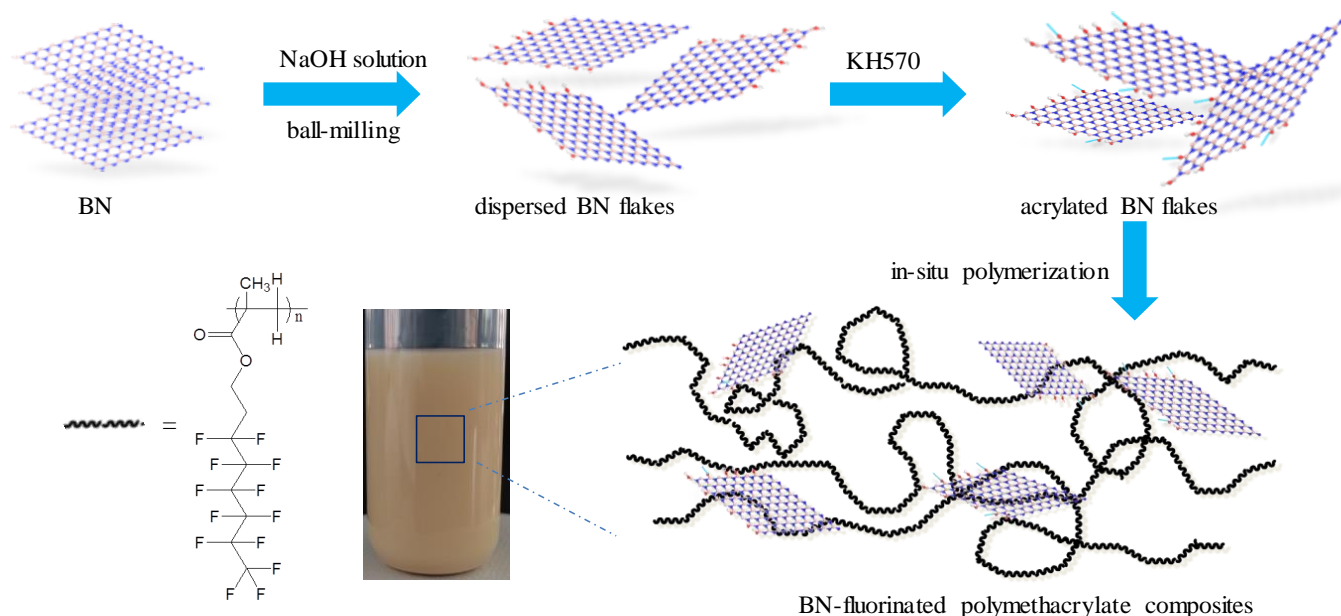
2. Material and Methods

2.1. Materials

Sodium chloride (NaCl) and boron nitride (BN) were purchased from Aladdin Chemical Co. Ltd., Shanghai, China. 3-(Trimethoxysilyl)propyl methacrylate (KH-570) was acquired from Yuanye Biological Technology Co. Ltd., Shanghai, China. Butyl acetate (BAC) and azodiisobutyronitrile (AIBN) were purchased from J&K Scientific Ltd., Shanghai, China. Hydrofluoroether 1-(ethoxy)nonafluorobutane (HFE-7200) was purchased from 3M China. 2-(perfluorohexyl)ethyl methacrylate (C6Rf) was supplied by Beijing Thinvec Co. Ltd., Beijing, China. Before experiments, all of the copper sheets and Q235 steel sheets were cleaned in an ultrasonic bath for several times in a sequence of acetone, anhydrous ethanol, and deionized water. AIBN was purified by recrystallization prior to use, while other reagents were used as-received.

2.2. In Situ Polymerization

The in situ polymerization process is illustrated in Scheme 1. A horizontal planetary milling was used for dispersion of BN, according to ref. [27]. In a typical run, 2 g of micron-sized BN powder mixed with 2 M aqueous NaOH solution were loaded into a stainless steel grinding bowl with steel balls. The BN/NaOH solution mixture was milled for 24 h. The ground product was rinsed with HCl solution and repeatedly washed with deionized water until the pH was close to neutral. After the sample was dried, it was dispersed in IPA and sonicated at 45 kHz for 1 h. Then, 2.5 g KH-570 and 0.4 g ammonia water were added, sonicated at 45 kHz for 1 h, followed by stirring at 60 °C for 12 h. The product was centrifuged at 2000 g for 10 min and the top 3/4 of the supernatant was filtered to recover the final product. The acrylated BN flakes was referred to as BN570.



Scheme 1. Dispersion, acrylation of BN flakes and in situ polymerization to the PFPB composite coatings.

AIBN (0.085 g), C6Rf (5 g), KH-570 (0.287 g), BN570, BAC (15 g) were added into a polymerization tube. After purged with N₂, the mixture was heated at 70 °C for 24 h for polymerization. Then, the precipitate was collected, washed with ethanol and dried. The prepared BN-fluorinated poly methacrylate was referred to as PFBP-1, PFBP-2 and PFBP-3, according to the amount of BN570 of 0.045, 0.075 and 0.105 g, respectively. As a comparison, fluorinated poly methacrylate was synthesized through the same recipe but no BN was added, which was referred as to PF.

2.3. Preparation of Coating

The PFBP was dissolved in HFE-7200 to prepare coating solutions with concentrations of 1, 2.5 and 5 wt.%, which are referred to as 1PFBP, 2.5PFBP and 5PFBP, respectively. The PFBP composite was coated on Q235 carbon steel sheets or copper sheets by a simple casting method. After dried at room temperature, the test specimens were further treated in an oven at 80 °C for 3 h. The thickness of the coating was regulated by dropping 0.5 mL of the coating solution onto an O-ring circled area of the substrate.

2.4. Characterization

Fourier transform infrared (FTIR), and attenuated total reflection Fourier transform infrared (ATR-FTIR) spectra were collected using a Nicolet iS50 (Nicolet, Madison, WI, USA). Scanning electron microscopy (SEM) images were acquired on Hitachi S-4800 field emission scanning electron microscope (Hitachi, Tokyo, Japan) with an acceleration voltage

of 10 kV. The static water contact angle (WCA) was measured using an optical contact angle meter (Dongguan Sindin SDC-100, Shengding, Dongguan, China).

2.5. Electrochemical Polarization Measurements

Electrochemical polarization measurements were performed on a CHI-604E, Chenhua electrochemical instrument (Chenhua, Shanghai, China). A three-electrode configuration was employed with the test specimen as the working electrode, a Pt plate as the counter electrode, and a saturated calomel electrode (SCE) as the reference electrode. The working electrode had an area of 1 cm², opening to 3.5 wt.% NaCl solution as the electrolytic solution. Prior to the measurements, the working electrode was immersed in the electrolytic solution for 20 min to establish a stable open circuit potential (OCP). Electrochemical impedance spectroscopy (EIS, Chenhua, Shanghai, China) measurements were carried out with the frequency range of 10⁻²~10⁵ Hz with alternating current signals. Zview software (version 3.10) was used for analyzing the EIS results within an error of 10%.

2.6. Adhesion Test

The adhesion between the coating and the substrate was tested according to Adhesion Test Procedure-ASTM 3359 [28]. In a typical run, the cutting tool was put on the coated copper sheet. The tool was pressed down and pulled to create a cross hatch pattern. Then, the coating was covered with 3M Scotch tape and the tape was smoothed so that it fitted closely with the coating. The tape was removed by pulling in a single smooth action at an angle of 180°. Finally, the surface of coating was inspected by a microscope to evaluate the adhesion by comparing with the ASTM description.

2.7. Abrasion Resistance Test

The abrasion resistance test was according to a simplified procedure of ISO 7784-2. The PFBP-coated specimen was loaded with a 60 g counterweight covered by non-woven cloth. Then, the counterweight was horizontally moved for various times. The abrasion resistance was evaluated by monitoring the water contact angle and the Tafel curves.

2.8. Salt Fog Corrosion Test

Prior to the corrosion tests, Q235 carbon steel with a working area of 5 cm² was rinsed with acetone and ethanol in an ultrasonic bath and dried in air. Then, the carbon steel was coated with PFBP composites. After cured at 80 °C for 3 h, the coated substrate was exposed in a salt spray. The salt fog test was carried out at a constant temperature of 35 °C, and the corrosion was recorded periodically [29].

3. Results and Discussion

The as-received BN powder exhibits morphology of particle, confirmed by the SEM and TEM images (Figure 1A,C). After the wet-milling with the NaOH solution followed by modification with KH-570, the morphology of the acrylated BN (BN570) becomes aggregates of BN flakes (Figure 1B). The dispersion of the BN flakes are further verified by the TEM image (Figure 1D). The well-dispersed BN flakes are beneficial to copolymerize with the fluorinated acrylate monomer and formed stable coating solution.

3.1. Sedimentation of Coating Solution

UV-vis spectrophotometry based on the Lambert–Beer law indicates that the absorbance is linearly related to the concentration of a solution [30]. As a result, the sedimentation of the PFBP coating solution can be evaluated by monitoring the absorbance and the sedimentation data are collected in Table S1. Here, 5 wt.% BN dispersed in HFE-7200 suspension shows a severe sedimentation with a settlement rate of about 84.9% after settling for 24 h. After BN is exfoliated and modified by KH-570, the value is greatly reduced to 16.7%. Furthermore, after the in situ polymerization, the as-prepared 5PFBP-2 coating solution (5 wt.%) shows a negligible settlement rate of 0.76%. The prepared BN-fluorinated

polymethacrylate coating solution is quite stable, which is beneficial to the formation of uniform coating with high performance.

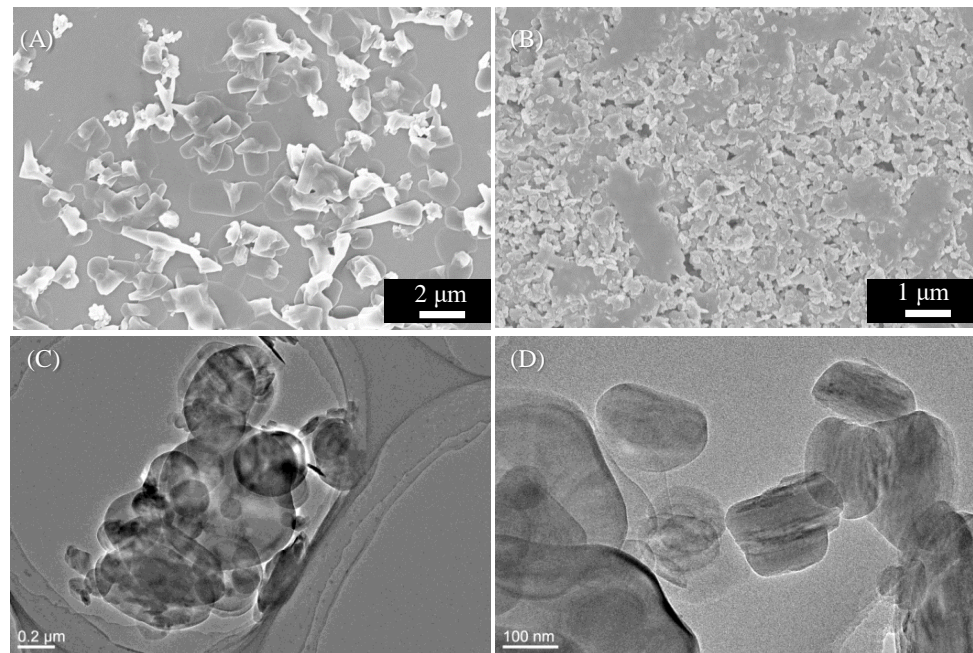


Figure 1. SEM and TEM images of BN (A,C) and BN570 (B,D).

3.2. Coating Composition

Figure 2a shows the FTIR spectra of KH-570, BN570, and BN. Two broad peaks at 1231 and 737 cm^{-1} can be observed, corresponding to the absorption bands of BN [25]. While the KH-570 modification of BN570 shows additional peaks at $2840\sim 2950$, 1640 and 1723 cm^{-1} , which are attributed to C–H, C=C and C=O, respectively. FTIR spectra confirm that the C=C bond has been successfully grafted on BN, providing the moiety for the in situ polymerization. ATR-IR spectra of the PFBP coatings present peaks at 1723 and $1400\text{--}1000\text{ cm}^{-1}$, which are associated with the bond of C=O and C–F [31], respectively (Figure 2b). Additionally, absorption peak at 1640 cm^{-1} attributing to the stretch vibration of C=C disappears, indicating the completion of polymerization. However, the characteristic peaks of BN at 1231 and 737 cm^{-1} are not well resolved due to their very low content and thus being masked by the peaks of polymer.

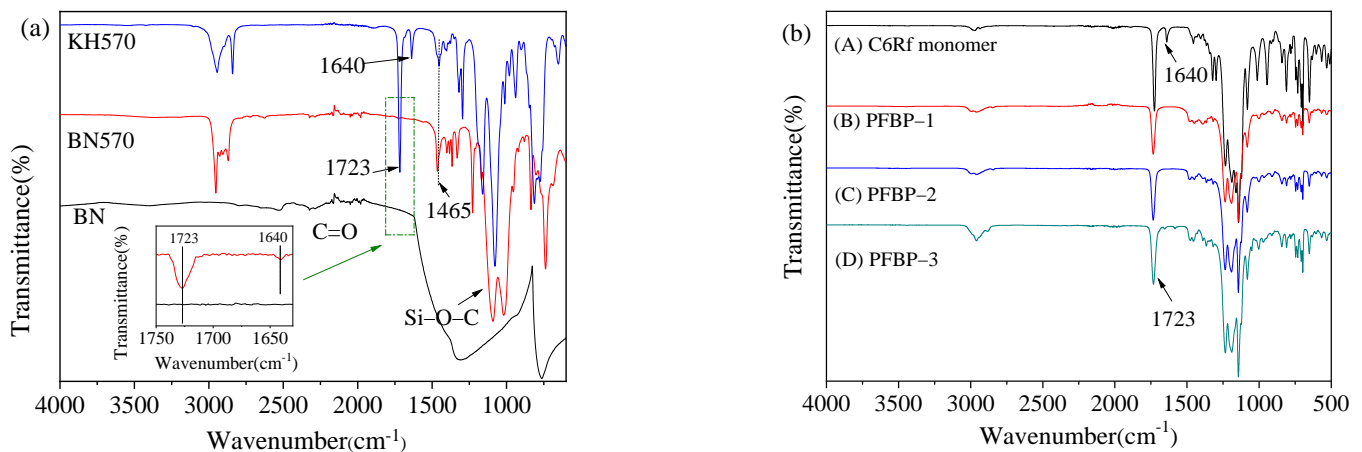


Figure 2. (a) FTIR spectra of KH570, BN570, and BN, inset is the enlargement of rectangle; (b) ATR-IR spectra of C6Rf monomer (A), PFBP-1 (B), PFBP-2 (C) and PFBP-3 (D).

3.3. Microstructures

From top-view of the PFBP coatings (Figure 3), one can see that the formed PFBP coatings are dense and flat. Some BN flakes are observed when increasing the content of BN570 in PFBP. Cross-sectional images indicate that all the coatings are uniform in thickness. PFBP-1, PFBP-2 and PFBP-3 coatings prepared from 1 wt.% coating solution show slightly increased thickness of 363, 394 and 414 nm, possibly due to the increase in the BN570 content. Additionally, an increase in the coating solution concentration leads to a thicker film. PFBP-2 coating solutions with concentrations of 2.5 wt.% and 5 wt.% produce coatings with thickness of 578 and 726 nm, respectively. The coating were peeled off from the substrate and embedded in a resin to obtain cross-sectional slices. It can be seen that the BN sheets (indicated by circles) are well distributed in the coatings (Figure 3F,G). The surface wettability of the coatings is tested by the measurements of water contact angle (WCA). All the PFBP coatings show hydrophobicity with close WCA around 110° (Figure 3, inset). The side chains of -CF₂ connected to the main chain of acrylate through ester bonds contribute to the good hydrophobicity.

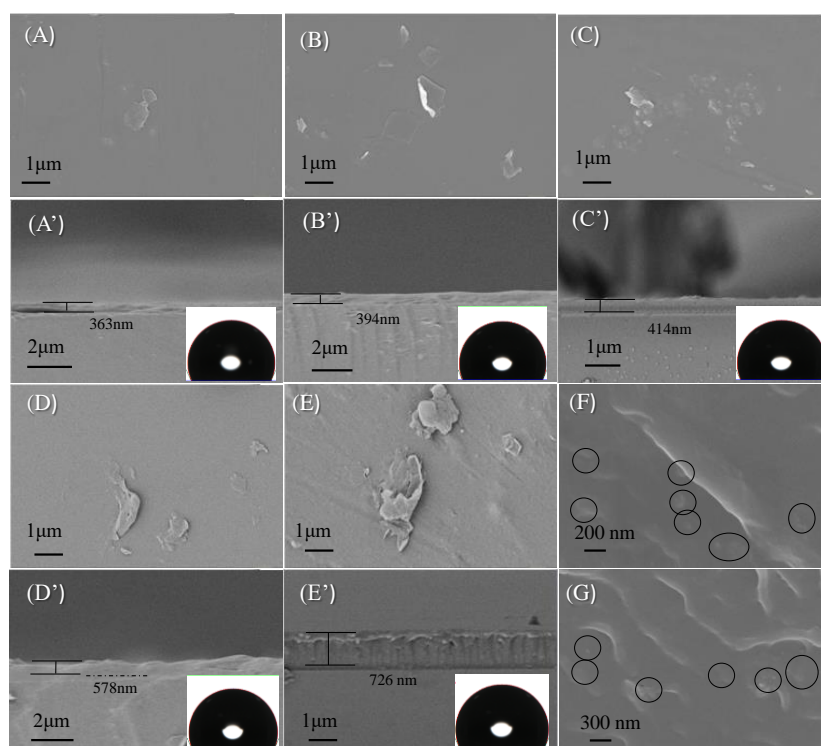


Figure 3. SEM images of top-view (A–E) and cross-section (A'–E') of PFBP coatings prepared from different coating solutions. (A,A') 1 wt.% PFBP-1 coating solution; (B,B') 1 wt.% PFBP-2 coating solution; (C,C') 1 wt.% PFBP-3 coating solution; (D,D') 2.5 wt.% PFBP-2 coating solution; (E,E') 5 wt.% PFBP-2 coating solution. Insets are photographs of water drop on the corresponding coatings; and cross section images of coating slices (F,G). The slices were prepared by embedding coatings in Technovit®7100.

3.4. Electrochemical Corrosion Test

Electrochemical polarization is a conventional method to evaluate the corrosion resistance of coatings. A lower self-corrosion current density (I_{corr}) means a slower corrosion rate. As shown in Figure 4, the Tafel curve of the PF coated Cu sheet evidently shifts to the lower right corner, compared to that of the bare Cu sheet. This indicates that coating with fluorinated polymer greatly improves the corrosion resistance. PF coating with good hydrophobicity prevents the corrosive medium (3.5 wt.% NaCl aqueous electrolyte) from contacting the Cu substrate and thus inhibits the corrosion. By contrast, the Tafel curves of

the BN incorporated PFBP coatings are positioned lower than that of the PF coating, which means that PFBP coatings display better corrosion resistance than the PF coating. When increasing the thickness of the coatings by using higher concentration coating solution, the Tafel curves further move to a lower position, implying the achievement of better corrosion resistance performance. Corrosion data fitted from the Tafel curves are collected in Table 1. I_{corr} of PFBP-1, PFBP-2 and PFBP-3 coatings are remarkably decreased to be 0.05, 0.018 and $0.074 \mu\text{A}\cdot\text{cm}^{-2}$, respectively, much lower than that of bare Cu sheet and PF. It is also observed that all of the PFBP coating samples exhibit a maximum corrosion rate lower than $8.6 \text{ mm}\cdot\text{year}^{-1}$, much slower than that for PF coating. Additionally, corrosion potential (E_{corr}) also indicates the corrosion trend. The more positive the E_{corr} is, the more difficult the corrosion inclines to be. The Tafel curves for the PFBP-coated Cu sheet give an E_{corr} higher than -171 mV , more positive than for bare Cu sheet and PF at -290 and -226 mV , respectively. Among the PFBP-2 coatings with different thickness, it can be observed that 5PFBP-2 shows the best corrosion resistance. The I_{corr} for 5PFBP-2 is $0.4 \text{ nA}\cdot\text{cm}^{-2}$, which decreases two orders of magnitude compared to the 1PFBP-2.

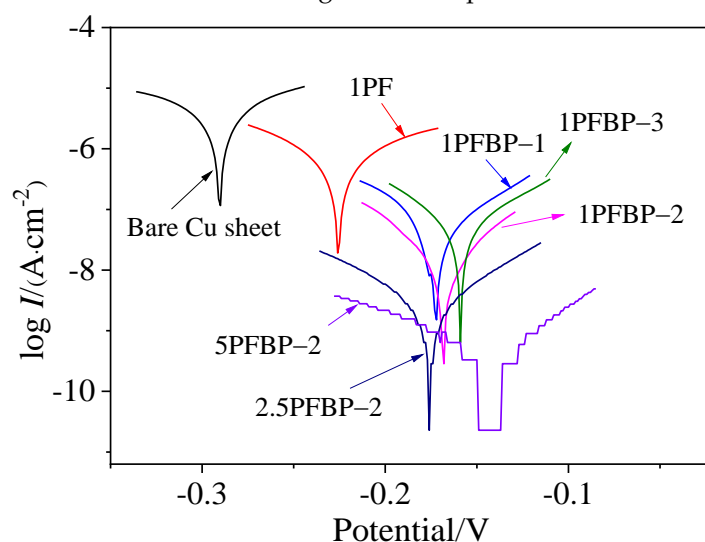


Figure 4. Tafel curves for bare Cu sheet and various coatings on Cu sheet.

Table 1. Electrochemical corrosion data from Tafel curves.

Coating	$I_{\text{corr}}/(\mu\text{A}\cdot\text{cm}^{-2})$	$E_{\text{corr}}/\text{mV}$	$R/10^{-4} (\text{mm}\cdot\text{year}^{-1})$
Bare Cu sheet	16.5	-290	—
1PF	1.86	-226	220
1PFBP-1	0.050	-171	5.70
1PFBP-2	0.018	-168	2.10
1PFBP-3	0.074	-159	8.60
2.5PFBP-2	0.004	-176	0.42
5PFBP-2	0.0004	-153	0.05

Note: I_{corr} : corrosion current; E_{corr} : corrosion potential; R : corrosion rate.

The electrochemistry corrosion behavior of the 5PFBP-2 coating is further investigated by analyzing the EIS data acquired through immersing the samples in 3.5 wt.% NaCl solution for 20 min, 16 h, 24 h, and 72 h, respectively, and the results are shown in Figure 5. After 16 h of immersion, the impedance of the 5PFBP-2 coated sample declines a little but the shape of Bode plots does not change and still keeps one time constant. Therefore, the curves can be fitted by the equivalent circuit model in Figure 5b. This indicated that the composite coating was effective in protecting the metal substrate from corrosion after even 16 h of immersion. With a prolonged immersion time of 24 h, two time constants appeared in the phase angle diagram and no longer conformed to the aforementioned equivalent circuit. Instead, the equivalent circuit model 2 in Figure 5b was used for fitting. The time

constant at high frequency corresponds to the barrier performance of the coating [14,32], while the occurrence of one at low frequency indicates that the metal substrate has a corrosion reaction due to the infiltration of the corrosion medium [33,34]. Here, R_{ct} is the charge transfer resistance between the substrate and the electrolyte, CPE2 is the constant phase angle elements representing capacitive properties of the electric double layer. It can be seen that the EIS data are well fitted by the models. The fitted data are collected in Table S2. After 72 h of immersion, the R_c of the coating decreased by near three orders of magnitude compared to the one immersed for 20 min (Figure S1), indicating that the electrolyte penetrates across the coating and corrodes the metal substrate.

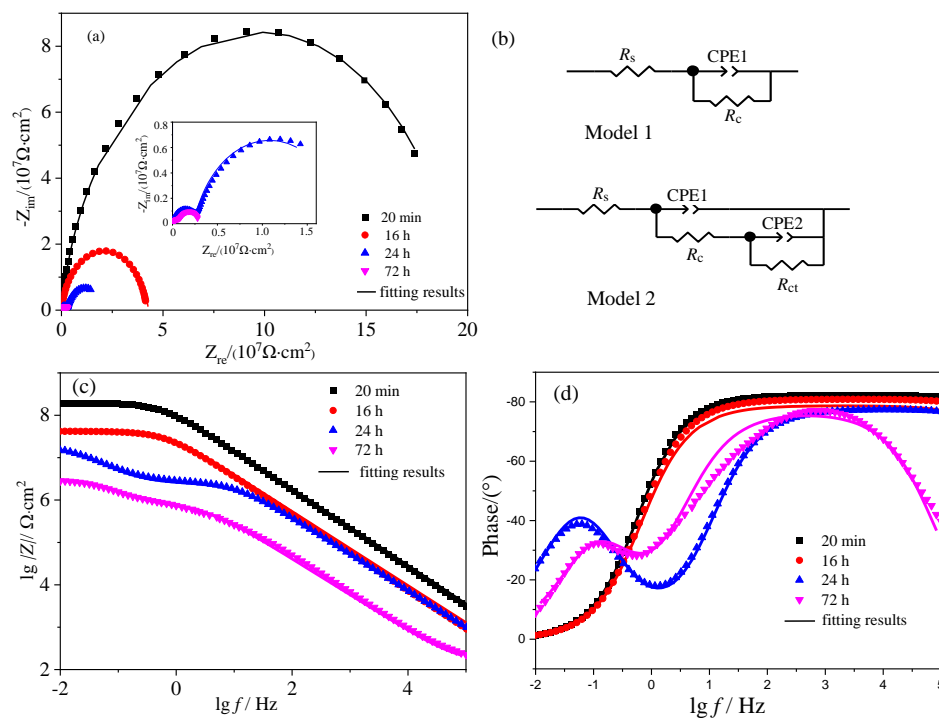


Figure 5. Nyquist (a) and Bode (c,d) plots of 5PFBP-2 coating immersed in 3.5 wt.% NaCl solution for different time, and the equivalent circuits used for fitting the Nyquist plots (b).

The electrochemical impedance spectra (EIS) measurements were used to investigate the electrochemical behaviors of bare Cu sheets and PFBP-coated samples. Figure 6 illustrates the Nyquist and Bode plots of the different coatings tested in NaCl solution (3.5 wt.%) at room temperature. The Nyquist plots construct a semi-circle, indicating that the electrode process is determined by the electrochemical step. The capacitive arc radius becomes remarkably larger after the Cu sheets are coated by the PF (Figure 6a, inset). The arc radius is even bigger when increasing the content of BN flakes. However, PFBP-3 with the highest BN content shows a reduced capacitive arc radius, indicating that excessive BN addition might deteriorate the barrier effect of the coating system [35]. This deteriorative trend is related to the aggregation of excessive fillers, supported by the SEM analysis results shown in Figure 3. For the PFBP-2 coatings, the thicker the coating is, the larger the capacitive arc radius is (Figure 6b). The impedance modulus at the lowest frequency ($Z_f = 0.01$ Hz) in Bode plot could be used as a semi-quantitative indicator of coating's barrier performance [32]. The values of coatings at $Z_f = 0.01$ Hz are collected in Table 2. Z_f values of PFBP are much higher than that of PF coating and bare copper sheet. Additionally, when increasing the thickness of PFBP coatings, the values at $Z_f = 0.01$ Hz are increased accordingly and improved to be $1.55 \times 10^8 \Omega \cdot \text{cm}^2$ for the 5PFBP-2 coating. The EIS data were fitted by model 1 in Figure 5b, where the R_c represents the charge transfer resistance, R_s is the solution resistance, and CPE1 is Constant Phase Angle Element 1. The fitted R_c values are summarized in Table 2. The R_c value is $25.06 \times 10^4 \Omega \cdot \text{cm}^2$ for the coating of 1PF.

While for the coating of 1PFBP-1, the value of R_c rises sharply and finally reaches up to $209.44 \times 10^4 \Omega \cdot \text{cm}^2$ for 1PFBP-2. Additionally, an increase in the concentration of PFBP-2 coating to 5% leads to a larger R_c of $1.559 \times 10^8 \Omega \cdot \text{cm}^2$. These results confirm that the 5PFBP-2 composite coating offers the most effective protection among all coatings.

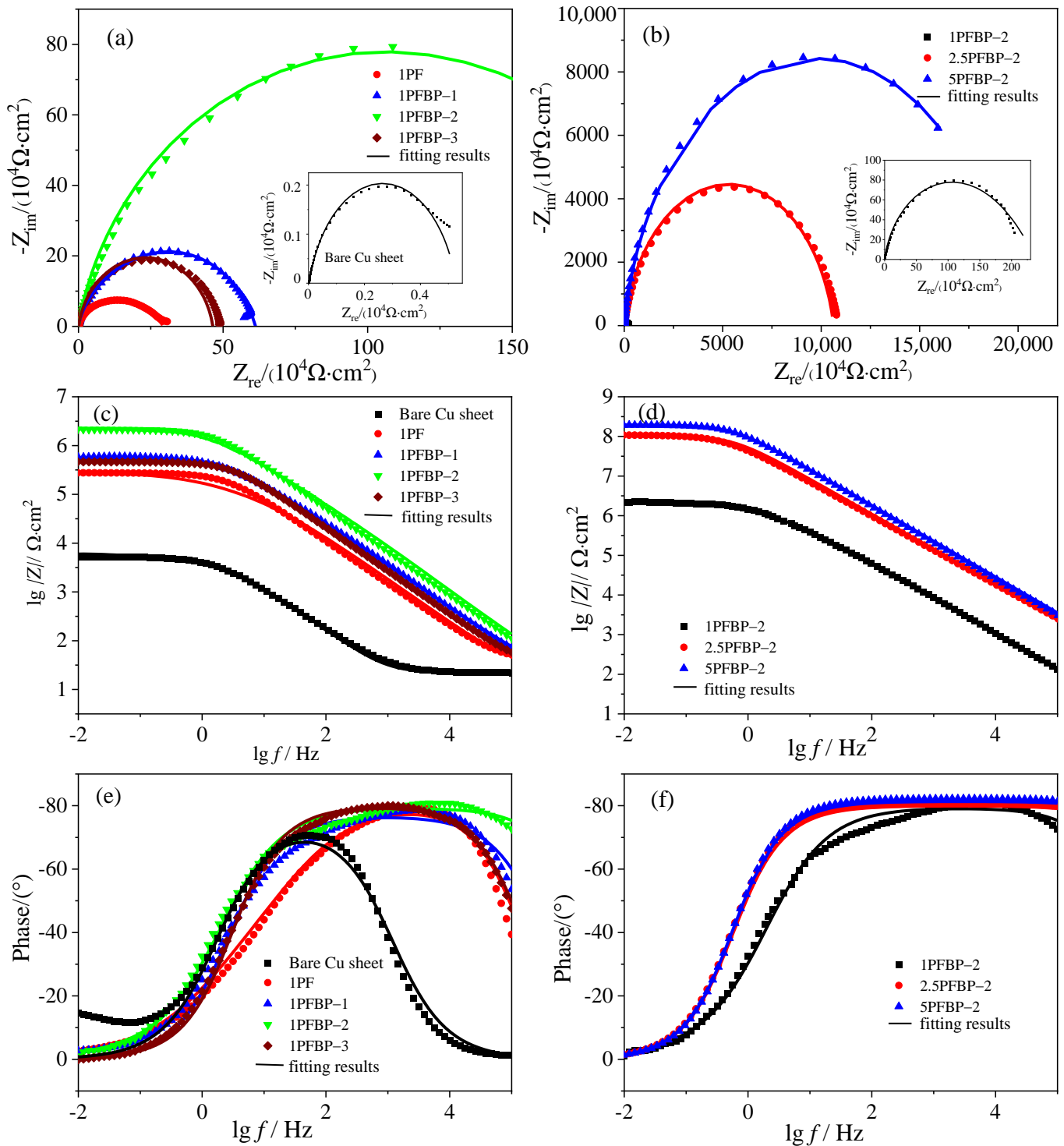


Figure 6. Nyquist (a,b) and Bode (c–f) plots of the different coatings in 3.5 wt.% NaCl aqueous solution.

Table 2. Fitting data of electrochemical AC impedance curve of PFBP coatings.

Sample	1PF	1PFBP-1	1PFBP-2	1PFBP-3	2.5PFBP-2	5PFBP-2
$R_c/(\Omega \cdot \text{cm}^2) \cdot 10^4$	25.06	55.77	209.44	48.00	14,480.00	15,590.00
$Z_{f=0.01 \text{ HZ}}/(\Omega \cdot \text{cm}^2)$	3.07×10^5	5.74×10^5	2.16×10^6	4.84×10^5	1.06×10^8	1.95×10^8

3.5. Surface Salt Fog Corrosion Test

Salt fog test was conducted to investigate the corrosion behaviors in intensified conditions. Q235 carbon steel is conventionally used as the substrate [36–39]. From the photographs, the appearance of the Q235 sheet shows no change after coating with PFBP. The evolution of the salt fog corrosion is illustrated in Figure 7. Corrosion easily happens on the bare substrate. By contrast, when the carbon steel sheets were coated with PFBP coatings, the corrosion was inhibited. The large area rust changes to be corrosion dots. Close inspection of three samples of 1PFBP-1, 1PFBP-2, 1PFBP-3 after 24 h of salt fog corrosion indicates that the Q235 sheet coated with 1PFBP-2 displays fewer corrosion dots. The 1PFBP-2 coating shows the best protective performance among the three coatings with different BN contents. For the 5PFBP-2 coating prepared with increased concentration of 5 wt.%, corrosion can be hardly observed even after 24 h of salt fog test, indicating the good corrosion resistance of the PFBP coating.

The morphology of the substrate after the salt fog tests was monitored by SEM technique. As shown in Figure 8, the Q235 carbon steel exhibits a flat surface with some orientation streaks. The orientation streaks can still be observed on the PFBP-coated Q235, suggesting the coating is very thin. After enduring a salt fog test for 18 h, severe corrosion occurs for the bare Q235 carbon steel. Many pits appear on the surface, indicating the pitting corrosion happens in the salt fog. By contrast, no change is observed for the PFBP-coated carbon steel, suggesting the good corrosion resistance of the PFBP coating.

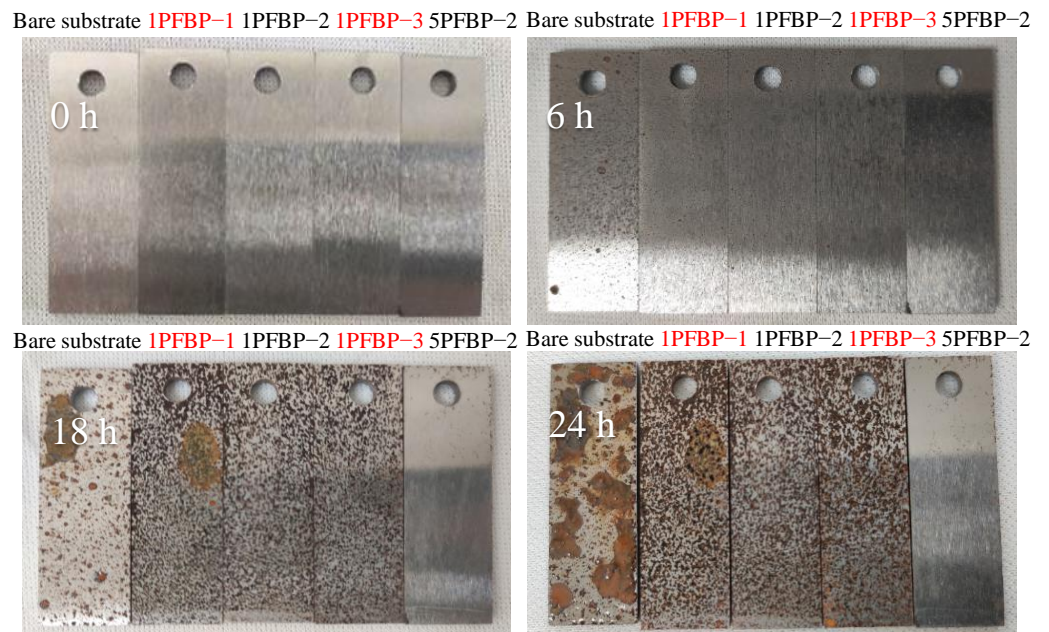


Figure 7. Photographs of Q235 carbon steel sheets coated with PFBP polymers after salt fog corrosion for different periods. From left to right: bare, 1PFBP-1, 1PFBP-2, 1PFBP-3 and 5PFBP-2.

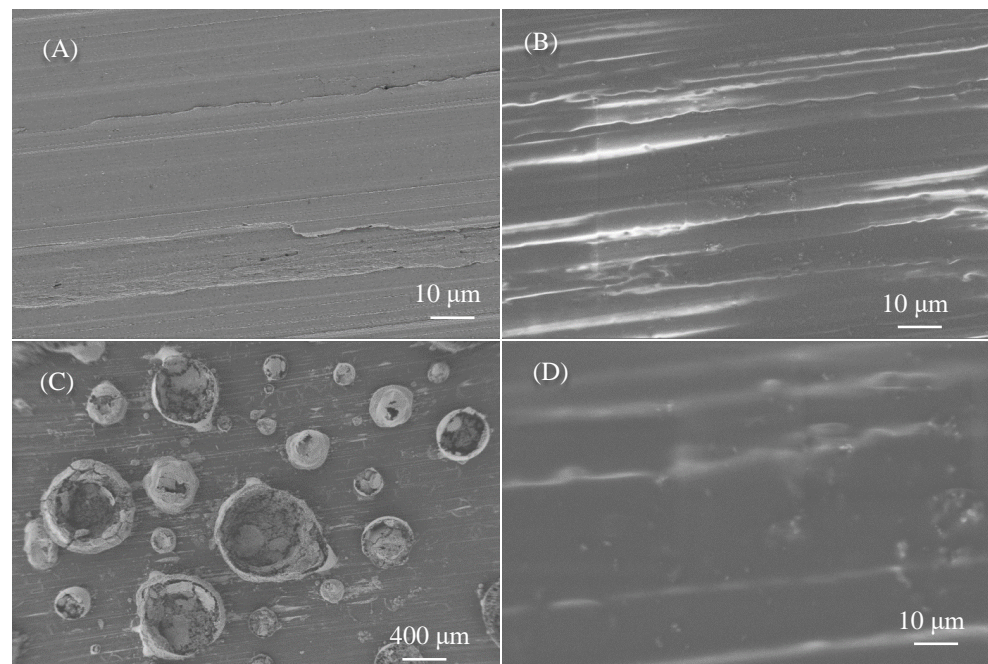


Figure 8. SEM images of bare Q235 carbon steel (A), Q235 carbon steel coated with PFBP-2 (B), bare Q235 carbon steel after salt fog test (C) and PFBP-2 coated Q235 carbon steel after salt fog test (D).

3.6. Adhesion Test

Adhesion test was performed on two different substrates coated with three coatings of 1PFBP-1, 1PFBP-2 and 1PFBP-3, respectively. The micrographs of coatings after hundred cell tests are shown in Figure 9. It can be seen that the scratch edges of the cut are smooth and no shedding is observed, which can be classified to be 5B grade according to ASTM 3359 [28]. This indicates that the PFBP coatings show good adhesion property. The fluororous coating solution features very low surface tension and can achieve good wetting of the substrate. The C=O bond linked to the C–C main chain of the acrylate polymer intensifies the adsorption forces due to the Keesom's dipole effect, Debye's induced dipole effect and London's dispersion effect [40]. By virtue of the good adhesion of the acrylate polymer matrix, the PFBP coatings show excellent adhesion properties.

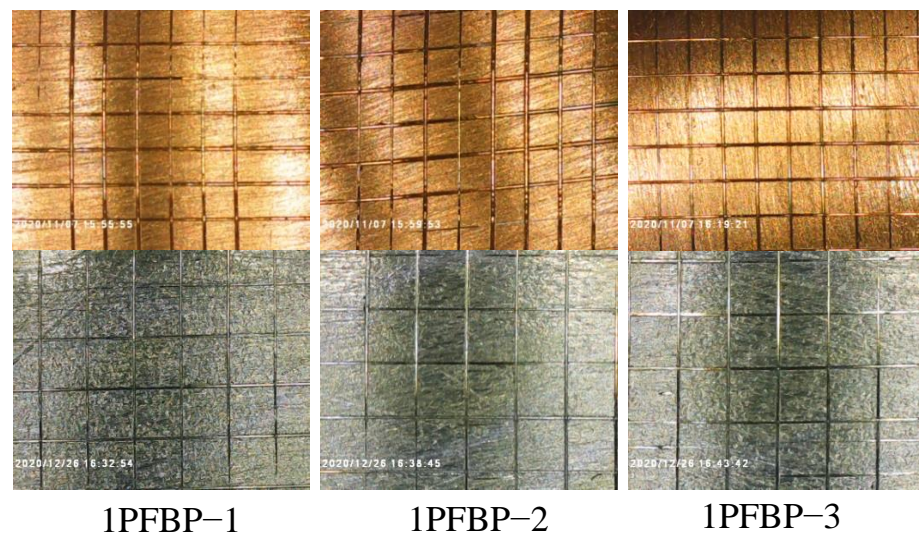
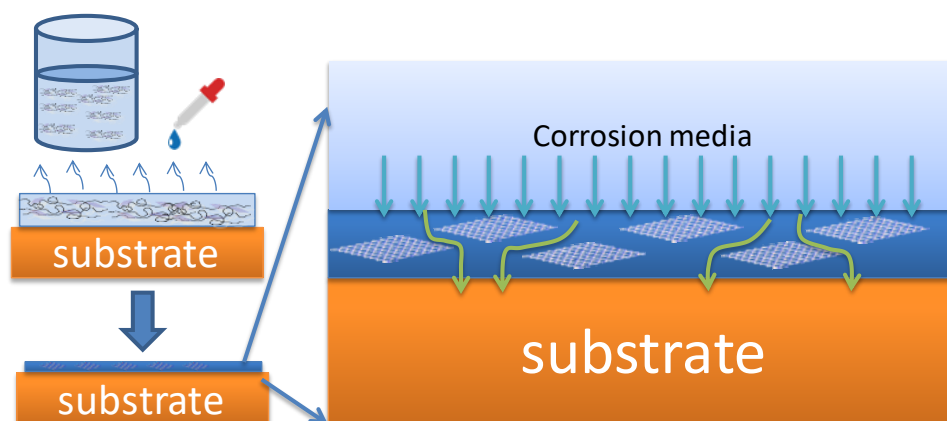


Figure 9. Micrographs of coatings on copper sheet (upper) and Q235 steel sheet (below) after hundred cell tests.

3.7. Abrasion Test of Coating

The abrasion resistance of the PFBP coating was studied through recording the water contact angle and Tafel curves after abrasion for hundreds of cycles. The Tafel curve and water contact angle of PFBP-2 coating after 400 cycles of abrasion exhibits a small change, compared to the one without abrasion (Figure S2). The corrosion potential and the corrosion current vary slightly, the corrosion rate only decays from 2.10 to 4.33 mm·year⁻¹ (Table S3). The evidences suggest that the PFBP coating features excellent abrasion resistance, which is plausibly attributed that the well-dispersed BN flakes are linked with the fluorinated poly methacrylate and reinforce the polymer chains.

As illustrated in Scheme 2, the coating solution containing well-dispersed BN-fluorinated poly methacrylate composites can be facily coated on substrate. After evaporation of the solvent, dense film forms which consists of BN flakes in the polymer matrix. In the case of bare substrate, electrochemical corrosion easily happens when the corrosion media directly contacts the substrate. The hydrophobic fluorinated poly methacrylate could separate the corrosion media from the substrate and thus delays the corrosion. For the coating of BN-fluorinated poly methacrylate composite, the combination of acrylated BN flakes and fluorinated acrylate through the in situ copolymerization, on one hand, improves the dispersion of BN flakes in the coating solution; on the other hand, it eliminates the voids between BN flakes and the polymer matrix. As a result, the penetration of the corrosion media from the coating film is greatly reduced and the labyrinth effect is intensified, compared to the composite coatings prepared by the physical incorporation of BN flakes [41].



Scheme 2. The formation of PFBP coatings and the corrosion resistance principle.

4. Conclusions

BN flakes, which were successfully prepared by wet-balling BN powder with NaOH solution, were modified with a silane coupling agent (KH570) to obtain acrylated BN flakes. The acrylated BN flakes were in situ copolymerized with 2-(perfluorohexyl)ethyl methacrylate to prepare BN-fluorinated poly methacrylate (PFBP) composites, which were well dissolved in a fluorous solvent. Beneficial from the chemical linkage between the BN flakes and the polymer chains, sedimentation seldom happens in the formed coating solution and BN flakes are well dispersed in the coating film. Electrochemical corrosion tests indicated that the corrosion resistance of the sample coated PFBP is greatly improved compared to the fluorinated polymethacrylate coating. The self-corrosion current density (I_{corr}) fitted from Tafel curves and the charge transfer resistance (R_c) derived from EIS of the PFBP-2 coating containing 2.5 wt.% BN are 0.018 $\mu\text{A}\cdot\text{cm}^{-2}$ and $2.09 \times 10^6 \Omega\cdot\text{cm}^2$, respectively. When increasing the concentration of PFBP-2, thicker coatings were prepared. The PFBP coating with 726 nm in thickness on Cu sheet displays I_{corr} and corrosion rate of as low as $4 \times 10^{-10} \text{A}\cdot\text{cm}^{-2}$ and $5 \times 10^{-6} \text{mm}\cdot\text{year}^{-1}$, respectively. Additionally, the PFBP coatings exhibit good adhesion to substrate and abrasion resistance, confirmed by adhesion and abrasion tests. The BN flakes dispersed in the fluorinated polymer act as

barriers for the penetration of corrosion media, improving the corrosion resistance of the coated samples. The prepared PFBP coating would find good applications in the corrosion protection of electronic devices through forming thin coating film.

Supplementary Materials: The following are available online at <https://www.mdpi.com/article/10.3390/coatings11121518/s1>, Figure S1: Pore resistance of the coating (R_c) for the specimen coated with 5PFBP-2 coating at different immersion time in 3.5 wt.% NaCl solution, Figure S2: Surface wettability (a) of 1PFBP-2 coating after numbers of friction and Tafel curves (b) of 1PFBP-2 coating after 400 cycles of abrasion, Table S1: Absorbance and calculated sedimentation rate of the coating solutions, Table S2: EIS fitting parameters of 5PFBP-2 coatings in various immersion times, Table S3: Electrochemical corrosion data from Tafel curves of 1PFBP-2 coating before and after friction for 400 cycles.

Author Contributions: Conceptualization, X.M. and Q.X.; methodology, Q.X.; software, Q.H.; validation, A.L.; formal analysis, Q.H. and A.L.; investigation, Q.H. and Y.W.; resources, Y.M.; data curation, Y.M. and H.Z.; writing—original draft preparation, Q.H.; writing—review and editing, H.Z. and Q.X.; visualization, Q.H. and Y.M.; supervision, Q.X.; funding acquisition, Q.X. All authors have read and agreed to the published version of the manuscript.

Funding: This research received no external funding.

Institutional Review Board Statement: Not applicable.

Informed Consent Statement: Not applicable.

Data Availability Statement: Not applicable.

Acknowledgments: Financial support by the Beijing Thinvec conjoint project is gratefully acknowledged.

Conflicts of Interest: The authors declare that they have no known competing financial interest or personal relationship that could have appeared to influence the work reported in this paper.

References

1. Hu, G.R.; Zhang, S.; Bu, F.J.; Lin, J.C.; Song, L.G. Recent progress in corrosion protection of magnesium alloys by organic coatings. *Prog. Org. Coat.* **2012**, *73*, 129–141. [[CrossRef](#)]
2. Vazirinasab, E.; Jafari, R.; Momen, G. Application of superhydrophobic coatings as a corrosion barrier: A review. *Surf. Coat. Technol.* **2018**, *341*, 40–56. [[CrossRef](#)]
3. James, G.R.; John, B.D. Fluorinated naval coatings. *Ind. Eng. Chem. Prod. Res. Dev.* **1978**, *17*, 8–9. [[CrossRef](#)]
4. Yin, X.; Song, Z.Y.; Liang, Y.Z.; Zhang, B.; Fang, F.L.; Zhu, P.L.; Zhu, K.B. Synthesis of sulfonyl fluorinated macro emulsifier for low surface energy emulsion polymerization application. *J. Appl. Polym. Sci.* **2017**, *134*, 44921. [[CrossRef](#)]
5. Imae, T. Fluorinated polymers. *Curr. Opin. Colloid Interface Sci.* **2003**, *8*, 307–314. [[CrossRef](#)]
6. Honda, K.; Morita, M.; Otsuka, H.; Takahara, A. Molecular aggregation structure and surface properties of poly (fluoroalkyl acrylate) thin films. *Macromolecules* **2005**, *38*, 5699–5705. [[CrossRef](#)]
7. Weng, J.C.; Peng, W.C.; Chang, C.H.; Chang, H.Y.; Yeh, M.J. Corrosion resistance conferred by superhydrophobic fluorinated polyacrylate-silica composite coatings on cold-rolled steel. *J. Appl. Polym. Sci.* **2012**, *126*, E48–E55. [[CrossRef](#)]
8. Liang, L.X.; Liu, H.C.; Mi, X.; Zhu, D.W.; Zhou, Q.; Xiao, Q. Preparation and corrosion resistance of SiO₂ or TiO₂ nano particles/fluorinated polyacrylate polymer composite coatings. *J. Compos. Mater.* **2019**, *37*, 1832–1840. [[CrossRef](#)]
9. Maria, S.; William, R.; Will, G.J.; Anna, Z.M.; Michael, C.F.; Alex, Z. Graphene as a long-term metal oxidation barrier worse than nothing. *ACS Nano* **2013**, *7*, 5763–5768. [[CrossRef](#)]
10. Kalendová, A.; Sapurina, I.; Stejskal, J.; Veselý, D. Anticorrosion properties of polyaniline-coated pigments in organic coatings. *Corros. Sci.* **2008**, *50*, 3549–3560. [[CrossRef](#)]
11. Liu, D.; Zhao, J.W.; Liu, S.; Cen, H.Q.; Xue, J.Q. Comparative tribological and corrosion resistance properties of epoxy composite coatings reinforced with functionalized fullerene C60 and graphene. *Surf. Coat. Technol.* **2016**, *286*, 354–364. [[CrossRef](#)]
12. Mo, T.M.; Zhao, J.W.; Chen, F.Z.; Yu, Y.Q.; Zeng, X.Z.; Wu, D.X.; Xue, J.Q. Excellent tribological and anti-corrosion performance of polyurethane composite coatings reinforced with functionalized graphene and graphene oxide nanosheets. *RSC Adv.* **2015**, *5*, 56486–56497. [[CrossRef](#)]
13. Zhang, R.X.; Ma, N.R.; Du, A.; Liu, Q.; Fan, Y.Z.; Zhao, X.; Wu, J.J.; Cao, M.X. Corrosion resistance of organic coating based on polyhedral oligomeric silsesquioxane-functionalized graphene oxide. *Appl. Surf. Sci.* **2019**, *484*, 814–824. [[CrossRef](#)]
14. Shen, T.L.; Zhao, D.Y.; Wang, Y.; Song, B.R.; Yao, Q.; Chen, S.S.; Chai, Y. A long-term corrosion barrier with an insulating boron nitride monolayer. *J. Mater. Chem. A* **2016**, *4*, 5044–5050. [[CrossRef](#)]
15. Eichler, J.; Lesniak, C. Boron nitride (BN) and BN composites for high-temperature applications. *J. Eur. Ceram. Soc.* **2008**, *28*, 1105–1109. [[CrossRef](#)]

16. Jiang, B.H.; Ma, T.L.; Yang, Q.; Tang, J.Z.; Song, F.X.; Zeng, B.H.; Zhi, Y.C. Three-dimensional porous boron nitride foam for effective CO₂ adsorption. *Solid State Commun.* **2019**, *294*, 1–5. [[CrossRef](#)]
17. Lin, Y.; Connell, W.J. Advances in 2D boron nitride nanostructures: Nanosheets, nanoribbons, nanomeshes, and hybrids with graphene. *Nanoscale* **2012**, *4*, 6908–6939. [[CrossRef](#)]
18. Lee, H.G.; Yu, J.Y.; Lee, C.; Dean, C.; Shepard, L.K.; Kim, P.; James, H. Electron tunneling through atomically flat and ultrathin hexagonal boron nitride. *Appl. Phys. Lett.* **2011**, *99*, 243114. [[CrossRef](#)]
19. Jiang, H.; Wang, Z.; Ma, L.; Yang, Q.; Tang, Z.; Song, X.; Zeng, H.; Zhi, C. Boron ink assisted in situ boron nitride coatings for anti-oxidation and anti-corrosion applications. *Nanotechnology* **2019**, *30*, 335704. [[CrossRef](#)]
20. Husain, E.; Narayanan, N.T.; Taha-Tijerina, J.J.; Vinod, S.; Vajtai, R.; Ajayan, M.P. Marine corrosion protective coatings of hexagonal boron nitride thin films on stainless steel. *ACS Appl. Mater. Interfaces* **2013**, *5*, 4129–4135. [[CrossRef](#)]
21. Huang, P.Z.; Zhao, J.W.; Zhao, C.W.; Ci, J.X.; Li, T.W. Tribological and anti-corrosion performance of epoxy resin composite coatings reinforced with differently sized cubic boron nitride (CBN) particles. *Friction* **2021**, *9*, 104–118. [[CrossRef](#)]
22. Cui, J.M.; Ren, M.S.; Chen, J.; Liu, S.; Zhang, G.G.; Zhao, C.H.; Wang, P.L.; Xue, J.Q. Anticorrosive performance of waterborne epoxy coatings containing water-dispersible hexagonal boron nitride (h-BN) nanosheets. *Appl. Surf. Sci.* **2017**, *397*, 77–86. [[CrossRef](#)]
23. Cui, J.M.; Ren, M.S.; Qin, L.S.; Xue, J.Q.; Zhao, C.H.; Wang, P.L. Non-covalent functionalized hexagonal boron nitride nanoplatelets to improve corrosion and wear resistance of epoxy coatings. *RSC Adv.* **2017**, *7*, 44043–44053. [[CrossRef](#)]
24. Pan, D.; Zhang, D.X.; Yang, G.; Shang, Y.; Su, M.F.; Hu, Q.; Patil, R.R.; Liu, H.; Liu, T.C.; Guo, H.Z. Thermally conductive anticorrosive epoxy nanocomposites with tannic acid-modified boron nitride nanosheets. *Ind. Eng. Chem. Res.* **2020**, *59*, 20371–20381. [[CrossRef](#)]
25. Oh, H.; Kim, J. Fabrication of polymethyl methacrylate composites with silanized boron nitride by in-situ polymerization for high thermal conductivity. *Compos. Sci. Technol.* **2019**, *172*, 153–162. [[CrossRef](#)]
26. He, Z.; Zhao, J.; Li, F.; Zhang, D.; Guo, F.; Guo, H.; Wang, X.; Hu, H. In Situ synthesis of polymer-modified boron nitride nanosheets via anionic polymerization. *Appl. Surf. Sci.* **2021**, *537*, 147966. [[CrossRef](#)]
27. Lee, D.; Lee, B.; Park, H.K.; Ryu, J.H.; Jeon, S.; Hong, H.S. Scalable exfoliation process for highly soluble boron nitride nanoplatelets by hydroxide-assisted ball milling. *Nano Lett.* **2015**, *15*, 1238–1244. [[CrossRef](#)] [[PubMed](#)]
28. American Society for Testing of Materials (ASTM). *ASTM D3359-02: Standard Test Methods for Measuring Adhesion by Tape Test*; ASTM: West Conshohocken, PA, USA, 2005.
29. American Society for Testing of Materials (ASTM). *ASTM B117-09: Standard Practice for Operating Salt Spray (Fog) Apparatus*; ASTM: West Conshohocken, PA, USA, 2009.
30. Tuckerman, B.L. On the intensity of light reflected from or transmitted through a pile of plates. *J. Opt. Soc. Am.* **1947**, *37*, 818–825. [[CrossRef](#)] [[PubMed](#)]
31. Zhao, Y.L.; Wei, Y.M.; Nie, J.; He, Y. Cationic UV-curable fluorine-containing polyacrylic epoxy prepolymer with good compatibility. *Prog. Org. Coat.* **2016**, *100*, 70–75. [[CrossRef](#)]
32. Conradi, M.; Kocijan, A.; Kek-Merl, D.; Zorko, M.; Verpoest, I. Mechanical and anticorrosion properties of nanosilica-filled epoxy-resin composite coatings. *Appl. Surf. Sci.* **2014**, *292*, 432–437. [[CrossRef](#)]
33. Sun, W.; Wang, D.L.; Wu, T.T.; Pan, Q.Y.; Liu, C.G. Synthesis of low-electrical-conductivity graphene/permanganate composites and their application in corrosion protection. *Carbon* **2014**, *79*, 605–614. [[CrossRef](#)]
34. Ye, H.X.; Lin, Z.; Zhang, J.H.; Zhu, W.H.; Liu, Z.; Zhong, L.M. Protecting carbon steel from corrosion by laser in situ grown graphene films. *Carbon* **2015**, *94*, 326–334. [[CrossRef](#)]
35. Liu, T.; Zhao, C.H.; Li, Y.J.; Zhang, W.D.; Zheng, R.W.; Wang, P.L. POSS-tetraaniline based giant molecule: Synthesis, self-assembly, and active corrosion protection of epoxy-based organic coatings. *Corros. Sci.* **2020**, *168*, 108555. [[CrossRef](#)]
36. Wu, Y.; Guo, L.; Tan, B.; Li, W.; Zhang, F.; Zheng, X. 5-Mercapto-1-phenyltetrazole as a high-efficiency corrosion inhibitor for Q235 steel in acidic environment. *J. Mol. Liq.* **2021**, *325*, 115132. [[CrossRef](#)]
37. Wang, J.; Liu, J.; Liu, Q.; Chong, Y. The inhibition performance of heterocyclic compounds on Q235 steel in methanol/formic acid medium: Experimental and theory. *J. Mol. Liq.* **2021**, *343*, 117663. [[CrossRef](#)]
38. Njoku, I.D.; Njoku, N.C.; Lgaz, H.; Okafor, C.P.; Oguzie, E.E.; Li, Y. Corrosion protection of Q235 steel in acidic-chloride media using seed extracts of Piper guineense. *J. Mol. Liq.* **2021**, *330*, 115619. [[CrossRef](#)]
39. Zhang, W.; Nie, B.; Wang, M.; Shi, S.; Gong, L.; Gong, W.; Pang, H.; Liu, X.; Li, B.; Feng, Y.; et al. Chemically modified resveratrol as green corrosion inhibitor for Q235 steel: Electrochemical, SEM, UV and DFT studies. *J. Mol. Liq.* **2021**, *343*, 117672. [[CrossRef](#)]
40. Poth, U.; Schwalm, R.; Schwartz, M.; Baumstark, R. *Acrylic Resins*; Vincentz Network: Hanover, Germany, 2011.
41. Cui, J.M.; Ren, M.S.; Qin, L.S.; Xue, J.Q.; Zhao, C.H.; Wang, P.L. Processable poly(2-butylaniline)/hexagonal boron nitride nanohybrids for synergetic anticorrosive reinforcement of epoxy coating. *Corros. Sci.* **2018**, *131*, 187–198. [[CrossRef](#)]